Reviewers' Comments to Authors:

Reviewer #2 :

General Comments:

This study applies the CART framework to the GLORYS12 reanalysis to diagnose global bottom-water return pathways, transformation, and ages. The topic is significant and the diagnostic framework is well suited to the problem. However, the manuscript in its current form contains several conceptual and methodological gaps that need to be addressed. My comments focus on: (1) the robustness of the CART implementation, particularly the treatment of diffusion and the numerical stability of the age computation; (2) the inconsistency between the conceptual schematic and the actual hotspot-based results; (3) the oversimplification of the forcing strategy and its implications for interpreting centennial-scale ages; and (4) the lack of attention to boundary and marginal-sea influences. I recommend **major revision**.

Response: We sincerely thank the reviewer for the careful and constructive assessment of our manuscript. The comments have helped us improve the transparency of the CART implementation, clarify the interpretation of the climatologically forced age diagnostics, and better align the conceptual framework, regional discussion, and diagnostic results. We believe these revisions have significantly strengthened both the methodology and the physical interpretation of the manuscript.

Specific Comments

1. The CART diffusion tensor and its implementation are insufficiently specified

The governing equations (Eq. 1) include an eddy-diffusivity term KTKT , which the authors state is estimated using the K-profile parameterization (Large et al., 1994). However, the manuscript does not specify how this diffusivity tensor is applied in the CART tracer equations:

1. Is KTKT applied as a purely vertical (diapycnal) diffusivity, or does it include horizontal/isopycnal components?
2. If the latter, what is the orientation of the diffusion tensor relative to the neutral density surfaces? This matters critically because diffusion along isopycnals (rather than across them) does not contribute to water-mass transformation but can still spread the bottom-water concentration signal, potentially biasing the diagnosed pathway structure.
3. Does the CART implementation use the same KPP mixing coefficients as the GLORYS12 native mixing scheme, or is it a separate offline diagnosis? This distinction affects whether the diapycnal exchange diagnosed in the tracer equations is dynamically consistent with the velocity field.

The authors should clarify these implementation details. If the diffusion tensor is not aligned with isopycnal surfaces, the diagnosed upward penetration of bottom-water signals could be artificially enhanced by horizontal/numerical diffusion rather than true diapycnal transformation.

Response: Thank you for this important comment. We agree that the original description of K_T as an eddy-diffusivity tensor was not sufficiently precise. In our CART implementation, K_T represents the vertical turbulent diffusivity used in the tracer equations. No explicit horizontal or isopycnal diffusivity is included. Therefore, the orientation of a horizontal diffusion tensor relative to the neutral-density surfaces does not arise in our formulation.

We also clarify the distinction between the native GLORYS12 mixing scheme and the diffusivity used in the offline CART calculation. The GLORYS12 reanalysis uses a turbulent kinetic energy (TKE) vertical-mixing scheme, whereas K_T in our CART calculation is diagnosed separately using the K-profile parameterization (KPP; Large et al., 1994). Thus, the CART tracer calculation uses the prescribed GLORYS12 velocity field together with an independently diagnosed vertical diffusivity, rather than reproducing the native GLORYS12 mixing closure. The KPP diffusivity does not modify the prescribed velocity field. The GLORYS12 native TKE mixing configuration is documented by the Copernicus Marine Service.

Importantly, the diapycnal velocity used in our analysis is diagnosed independently from the tracer diffusivity. It is calculated directly from the GLORYS12 velocity and neutral-density fields and does not depend on K_T. The concentration-weighted diapycnal flux subsequently combines this independently diagnosed diapycnal velocity with the CART concentration field. We have clarified these distinctions in the revised Methods.

The corresponding text now reads:

> *"where $\boldsymbol{u}$ is the three-dimensional velocity field from GLORYS12, z is the vertical coordinate, and K_T is the vertical turbulent diffusivity coefficient used in the offline CART calculation. K_T is estimated using the K-profile parameterization (KPP; Large et al., 1994) and enters the tracer equations only through the vertical diffusion terms in Eqs. (3a)–(3b); no explicit horizontal diffusivity is included. The KPP diffusivity is diagnosed separately from the native GLORYS12 mixing scheme and does not modify the prescribed GLORYS12 velocity field."*

We have also clarified the independence of the diapycnal-velocity diagnostic from the tracer diffusivity. The corresponding text now reads:

> *"This diapycnal velocity diagnostic does not directly use K_T and is calculated directly from the GLORYS12 velocity and neutral-density fields."*

2. Numerical stability of the water age computation in low-concentration regions

The water age is defined as A=T/C. This ratio becomes numerically unstable and physically meaningless where C approaches zero (e.g., in the upper ocean or far from source regions). The authors mention a concentration threshold of 0.05 to "identify regions effectively reached by bottom-water signals," but it is unclear how this threshold is applied to the age field:

1. Is the age masked where C<0.05, or is it still computed but flagged?
2. If masked, how does the masking affect the zonal-mean age distributions shown in Figure 6, particularly in the upper density classes where C is generally low?
3. More fundamentally, the ratio A=T/C is sensitive to small fluctuations in C; did the authors test the sensitivity of the age field to the choice of the lower concentration cutoff (e.g., 0.02 vs. 0.10)? A brief discussion or sensitivity test would be helpful.

Response: Thank you for this important comment. The original description of the $C = 0.05$ concentration threshold was unclear and could imply that this threshold was used to mask the water-age field. This was not the case. No finite lower-concentration mask was applied to the primary calculation of water age or to the age field shown in Fig. 6. The previously stated $C = 0.05$ threshold was not used in the subsequent age diagnostics, and we have therefore removed it from the revised manuscript.

We have also expanded the description of the CART age definition to clarify the meaning of $A = \Gamma/C$ in low-concentration regions. In the CART framework of Deleersnijder et al. (2001), C and Γ are respectively the zeroth and first moments of the local age-distribution concentration. Their ratio therefore represents the concentration-weighted mean age of the bottom-water-origin tracer present at a given location. Thus, for $C > 0$, A retains a defined physical interpretation even when the amount of tagged bottom-water tracer is small: it represents the mean age of that tagged fraction rather than the age of the full local water mass. We agree, however, that as C approaches zero, the ratio becomes increasingly sensitive to numerical uncertainty, and at $C = 0$ the water age is undefined. The revised Methods text now reads:

"Following the CART formulation of Deleersnijder et al. (2001), the age-distribution concentration of the bottom-water-origin tracer at location x and time t is represented by $c(x,t,\tau)$, where τ denotes tracer age. The bottom-water concentration C and age concentration Γ are respectively the zeroth and first moments of this age distribution,

$$C(x, t) = \int_0^{\infty} c(x, t, \tau)\, d\tau \qquad (1a)$$

$$\Gamma(x, t) = \int_0^{\infty} \tau\, c(x, t, \tau)\, d\tau \qquad (1b)$$

The water age is then defined as

$$A\ (x,\ t) = \frac{\Gamma\ (x,\ t)}{C\ (x,\ t)} = \frac{\int_0^\infty \tau\ c(x,\ t,\ \tau)\ d\tau}{\int_0^\infty c(x,\ t,\ \tau)\ d\tau} \qquad (2)$$

and therefore represents the concentration-weighted mean age of the bottom-water-origin tracer present at that location and time. It is used here to characterize the renewal timescale of bottom-water influence in Sect. 3.3."

We have further clarified the numerical treatment of the age calculation. Water age is evaluated only where $C > 0$. Locations with $C = 0$, together with numerically invalid age values, are assigned NaN and are excluded from subsequent diagnostics. The corresponding text added to Sect. 2.1 now reads:

"The diagnosed ages measure elapsed time for the tagged component under the repeated climatological annual cycle. Water age is diagnosed as $A = \Gamma/C$ only where $C > 0$. At locations where $C = 0$, or where the resulting age value is numerically invalid, A is assigned NaN and excluded from subsequent diagnostics."

We have also removed the previously stated $C = 0.05$ threshold. The corresponding description of the quasi-equilibrium criterion now reads:

"We therefore identify the local quasi-equilibrium time as the first post-arrival integration year at which the concentration tendency ($\partial C/\partial t$) falls below $10^{-3}\ yr^{-1}$. The annual-mean concentration and corresponding water age are sampled at this locally diagnosed time for subsequent analysis, so sampling times can differ among locations."

We have additionally clarified how the zonal-mean age field in Fig. 6 is constructed. The zonal averaging is applied directly to the locally diagnosed $A = \Gamma/C$ values, rather than by averaging C and Γ separately and subsequently taking their ratio; no additional weighting is applied. The corresponding statement added to the Fig. 6 caption reads:

"The zonal mean is calculated by directly averaging the locally diagnosed age $A = \Gamma/C$, rather than by averaging C and Γ separately; no additional weighting is applied."

Although no finite lower-concentration cutoff is used in the primary age diagnostic, we agree that the sensitivity of the age field to weak bottom-water signals should be assessed explicitly. Following the reviewer's suggestion, we therefore performed an additional post-processing sensitivity test using concentration thresholds of $C = 0.02$, 0.05, and 0.10. Relative to the original valid ocean volume, the retained volume fractions are 97.6%, 92.0%, and 74.5%, respectively. Thus, the $C = 0.02$ and 0.05 thresholds remove only a small fraction of the valid ocean volume, whereas the more restrictive $C = 0.10$ threshold excludes approximately one quarter.

To provide a stringent test of the age pattern, we further recalculated the zonal-mean water-age distribution after excluding all locations with $C < 0.10$. The result is shown in Fig. R1 below.

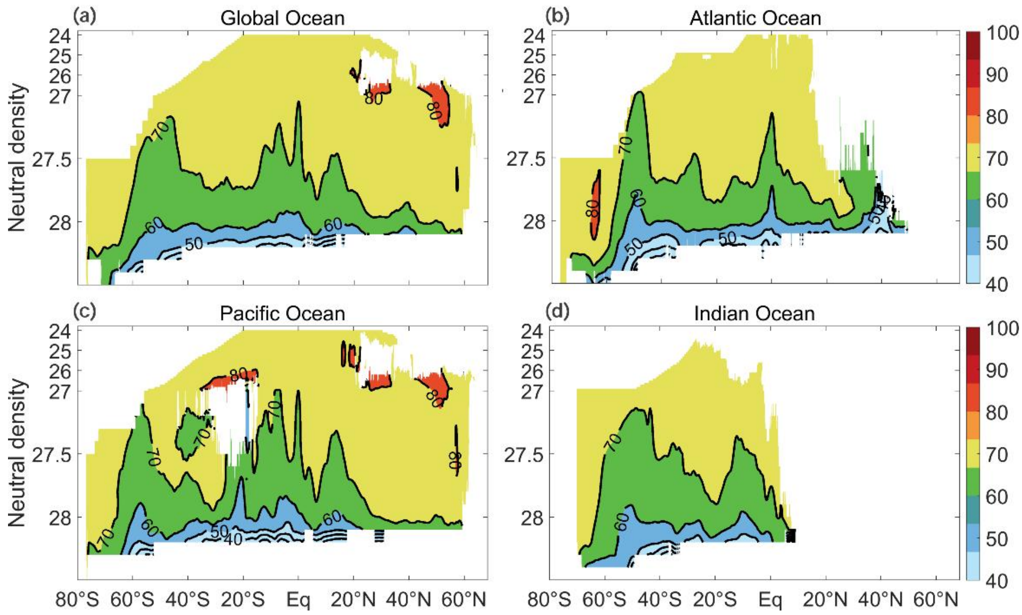

Figure R1. Zonal-mean bottom-water tracer age (years) after excluding locations with $C < 0.10$, for the (a) global ocean, (b) Atlantic Ocean, (c) Pacific Ocean, and (d) Indian Ocean.

The large-scale basin pattern remains evident after this relatively restrictive masking. In particular, the Pacific retains generally older tracer ages than the Atlantic and Indian Oceans, while the Southern Ocean continues to show the principal transition toward younger renewal signatures. However, many of the oldest-age regions are removed when locations with $C < 0.10$ are excluded. This comparison indicates that the broad basin-scale contrast is not generated solely by very weak bottom-water signals, whereas the spatial extent of the oldest diagnosed ages is more sensitive to the treatment of low-concentration regions.

We therefore retain the $C > 0$ age field as the primary diagnostic rather than imposing an arbitrary finite cutoff, while interpreting ages associated with very small C cautiously. The sensitivity experiment is used only as a post-processing robustness check and does not alter the definition of the primary age diagnostic.

To clarify the interpretation of the age diagnostic in very weak bottom-water-signal regions, we added the following text to the Discussion:

> *"A further consideration concerns the interpretation of water age where bottom-water concentration becomes very small. Within CART, $A = \Gamma/C$ represents the concentration-weighted mean age of the tagged bottom-water fraction present locally for $C > 0$. At $C = 0$, the age is undefined; these locations, together with numerically invalid age values, are assigned NaN and excluded from subsequent averaging. No finite lower-*

concentration cutoff is imposed in the primary age diagnostic, so positive C *values yielding valid* A *are retained. However, as* C *approaches zero, the ratio becomes increasingly sensitive to numerical uncertainty. We therefore assessed this sensitivity by applying post-processing concentration masks of* $C \geq 0.02$, 0.05, *and* 0.10, *which retain 97.6%, 92.0%, and 74.5% of the original valid ocean volume, respectively. Under the most restrictive* $C \geq 0.10$ *mask, the broad basin-scale age contrast remains evident, whereas many of the oldest-age regions are removed. Thus, the large-scale renewal pattern is retained under low-concentration masking, while the spatial extent of the oldest diagnosed ages is more sensitive to weak bottom-water signals and should be interpreted accordingly."*

3. The conceptual schematic (Figure 1) is at odds with the hotspot-oriented results

Figure 1 presents a schematic of bottom-water upward ventilation that appears to emphasize broad, diffuse diapycnal mixing and gradual upward spreading. However, the results in Figures 2–5 consistently emphasize that abyssal return is concentrated in localized topographic hotspots (Drake Passage, Kerguelen, Campbell/ridge sectors, equatorial Pacific) rather than being spatially homogeneous.

The schematic does not reflect this key finding. It shows relatively uniform isopycnal lifting and gradual lateral spreading, which aligns more with the classical Munk/Stommel view than with the "basin-dependent, hotspot-driven" structure the authors claim to have discovered. I recommend that the authors revise Figure 1 to explicitly illustrate the spatial heterogeneity of diapycnal mixing, perhaps by showing concentrated upwelling zones alongside broader along-isopycnal spreading, to better match their own diagnostic results.

Response: Thank you for this helpful comment. We agree that the previous conceptual schematic placed too much emphasis on broad upward spreading and did not sufficiently represent the spatially heterogeneous, hotspot-oriented structure diagnosed in Figs. 2–5. We have therefore substantially revised Fig. 1 to better reflect the physical organization identified in our results.

In the revised schematic, uneven bottom topography and localized zones of bottom-boundary-layer mixing and topographically enhanced internal-wave breaking are explicitly represented. These regions generate concentrated diapycnal upwelling and act as localized transformation hotspots. The mid-term state now shows bottom-water signals preferentially rising through these hotspots and forming spatially heterogeneous ventilation pathways, while broader along-isopycnal spreading is retained as a component of the subsequent interior redistribution. The late-integration state further illustrates the pathway-dependent increase in bottom-water ventilation timescales. The revised schematic is intended to represent this general hotspot-driven structure rather than individual geographic hotspots.

The revised Fig. 1 and its caption are shown below:

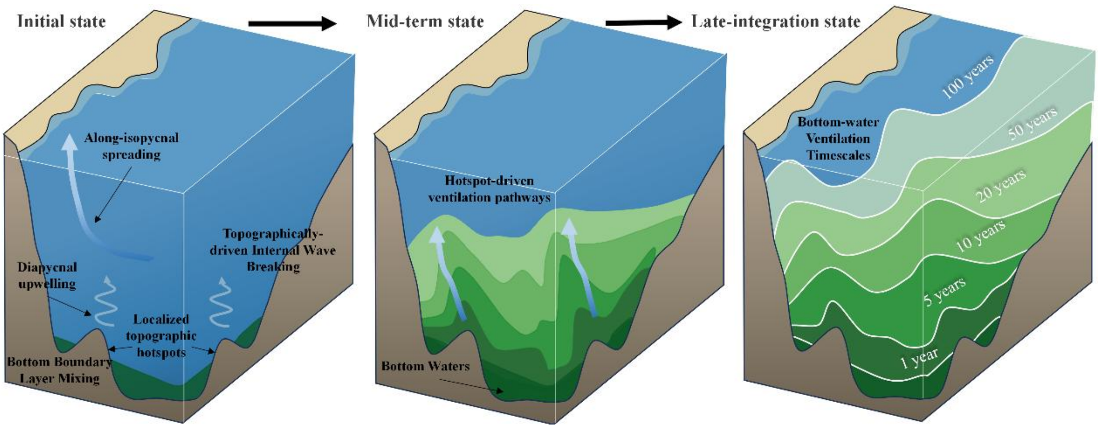

"Figure 1 Conceptual schematic of global bottom-water upward ventilation. In the initial state, dense bottom waters occupy abyssal layers. Bottom-boundary-layer mixing and topographically enhanced internal-wave breaking generate spatially localized zones of diapycnal upwelling, while bottom-water signals may spread more broadly along density surfaces. In the mid-term state, bottom-water signals preferentially rise through these localized hotspots and form spatially heterogeneous ventilation pathways into the ocean interior. In the late-integration state, bottom-water influence extends through the ocean interior, with ventilation timescales increasing away from source and transformation regions. The schematic emphasizes the coupled roles of localized diapycnal transformation, broader along-isopycnal spreading, and pathway-dependent renewal in organizing abyssal bottom-water return."

We have also revised the corresponding Introduction text to make the connection between the conceptual schematic and the diagnosed hotspot structure explicit. The revised text now reads:

"These processes imply that abyssal bottom-water return is organized around spatially localized transformation hotspots and preferential dynamical pathways rather than a single diffuse background upwelling field, as summarized schematically in Fig. 1."

4. The use of monthly climatological forcing and the interpretation of "centennial" ages

The CART simulation was forced with monthly climatological forcing derived from GLORYS12 (Line 112). This means that interannual-to-decadal variability (e.g., Southern Annular Mode, ENSO, decadal changes in AABW formation) is excluded. While this is a common simplification for tracer-age studies, it has important implications for interpreting the age field:

1. The ages shown in Figure 6 represent the climatological-mean renewal timescale, not the actual transient age that would result from the real ocean's varying forcing. The authors should state this clearly and avoid over-

interpreting the absolute age values (e.g., "70–80 years along the longer pathways") as if they were true calendar ages.

Response: Thank you for this important comment. We agree that the water ages diagnosed under monthly climatological forcing should not be interpreted as actual calendar ages in the time-varying ocean. Because the CART experiment is driven by climatological forcing, interannual-to-decadal variability is not represented, and the diagnosed ages are intended to characterize climatological renewal timescales of bottom-water return.

We have clarified this interpretation in the Methods. The corresponding text now reads:

> *"Using these initial and source-layer conditions, the CART equations are integrated continuously for 100 years under the monthly climatological forcing derived from GLORYS12. Here, the 100-year period denotes the model integration time under the climatological forcing rather than 100 calendar years of transient ocean evolution. The diagnosed ages measure elapsed time for the tagged component under the repeated climatological annual cycle."*

We have also clarified this interpretation when introducing the water-age results. The corresponding text now reads:

> *"We evaluate water age at the local sampling times selected by the concentration-tendency criterion in Sect. 2.1. These values represent the mean age of the tagged bottom-water fraction at those locations and sampling times within the 100-year integration. The zonal-mean distributions for the global ocean and the three major basins are shown in Fig. 6."*

Accordingly, the description of the Southern Ocean age values now reads:

> *"Age increases away from these sectors along the upward-spreading density pathways, with mean tracer ages of several decades and values of approximately 70–80 years in portions of the zonal-mean field. Previous trajectory-based estimates provide complementary context for these multidecadal values (Tamsitt et al., 2017)."*

The revised Fig. 6 caption now reads:

> *"Figure 6 Zonal-mean bottom-water tracer age (years), sampled at the locally diagnosed concentration quasi-equilibrium times defined in Sect. 2.1, in the (a) global ocean, (b) Atlantic Ocean, (c) Pacific Ocean, and (d) Indian Ocean. Shading represents the mean age of the tagged bottom-water fraction present at the selected sampling times, rather than a globally equilibrated age field."*

2. Does the 100-year integration length suffice for the Pacific abyssal regions, where ages appear to exceed 80–100 years in the northern interior? The age

field near the end of the integration may still reflect the initial conditions rather than a true steady state. The authors mention a quasi-equilibrium criterion ($\partial C/\partial t<10^{-3}$), but for regions with very slow renewal (e.g., North Pacific abyss), even this criterion may not guarantee full equilibration within 100 years. A more transparent discussion of this limitation is warranted.

Response: Thank you for this important comment. We agree that the 100-year integration does not necessarily allow the slowest abyssal regions to reach full equilibrium. The concentration-tendency threshold of $\partial C/\partial t<10^{-3}$ is used as a local operational criterion for identifying when the concentration field approaches a quasi-stable state; it should not be interpreted as evidence that the complete tracer-age field, particularly in slowly renewed abyssal regions, has reached a true steady state within 100 integration years.

This distinction is particularly important in the Pacific, where the diagnosed ages increase northward and locally approach the 100-year integration limit in the northern interior. We have therefore revised the corresponding Results text to make the finite integration window explicit. The revised text now reads:

"The Pacific exhibits the clearest contrast between pathway presence and temporal efficiency. Bottom-water influence clearly enters the basin from the south and remains visible in Fig. 4c, yet age increases rapidly northward and exceeds about 80 years over much of the basin, locally approaching the 100-year integration limit in the northern interior (Fig. 6c). These near-limit values should be interpreted as indicating very slow renewal within the finite integration window rather than as fully equilibrated abyssal ages."

We have also added an explicit discussion of this limitation in the Discussion section. In particular, we now clarify that the quasi-equilibrium criterion is a local concentration-based diagnostic and does not imply full equilibration of the tracer-age field throughout the abyssal ocean. The added text now reads:

"The 100-year CART integration also limits the interpretation of the slowest abyssal renewal. The concentration-tendency criterion provides a local measure of quasi-equilibrium, but satisfying this criterion does not imply that the complete tracer-age field has reached a steady state within the centennial integration. In slowly renewed abyssal regions, particularly in the northern Pacific, the bottom-water signal evolves on timescales comparable to or longer than the present integration window, and some locations may therefore remain transient at integration year 100. Ages approaching the 100-year limit in these regions should consequently be interpreted as evidence of very slow renewal within the diagnosed centennial window rather than as fully equilibrated abyssal ages. Longer integrations would be required to quantify their eventual equilibrium age structure and its subsequent evolution."

5. The role of marginal seas and overflows is neglected

The study focuses on the three major ocean basins, but bottom-water influence is also mediated by marginal seas (e.g., the Weddell Sea, Ross Sea, Nordic Seas) and by overflow pathways (e.g., through the Drake Passage, Scotia Sea, and various ridge gaps). The GLORYS12 reanalysis resolves these features, yet the paper does not discuss their contribution to the diagnosed return structure. For instance:

1. Does the ventilation thickness in the Weddell Sea sector (Figure 3) reflect local bottom-water formation/recirculation, or cross-isopycnal export?
2. Are the overflow pathways through the Romanche Fracture Zone or the Vema Channel in the Atlantic resolved in the concentration fields, and do they contribute to the Atlantic's "efficient upward penetration"?

Adding a brief discussion of these boundary and overflow influences would enrich the basin-comparative analysis and demonstrate that the authors have considered the full spectrum of return routes.

Response: Thank you for this helpful comment. We agree that marginal seas and narrow overflow passages provide important regional context for the basin-scale bottom-water return structure and were insufficiently discussed in the original manuscript.

Regarding the Weddell Sea, the enhanced ventilation thickness in Fig. 3 indicates a strong vertically integrated bottom-water influence in this sector. However, the present CART experiment continuously tags the model bottom layer globally rather than using separate regional source tracers. The Weddell Sea signal therefore cannot be uniquely partitioned into local bottom-water formation, gyre recirculation, export from the marginal sea, and subsequent cross-isopycnal transformation. We have clarified this distinction in the revised manuscript:

> *"The Southern Ocean continues to exhibit the largest and most coherent ventilation thickness, including pronounced signals near Drake Passage and the Weddell Sea, while secondary maxima emerge in the tropical-subtropical Pacific, along parts of the Atlantic western boundary system, and in the southern Indian Ocean. Because the global bottom layer is tagged uniformly in the CART experiment, the enhanced Weddell Sea signal reflects strong bottom-water influence in this sector but cannot by itself distinguish contributions from local formation and recirculation, export from the marginal sea, or subsequent cross-isopycnal transformation."*

Previous observational and modeling studies nevertheless establish the Weddell and Ross Seas as major formation and export regions of Antarctic Bottom Water and show that waters originating from different Antarctic sectors follow distinct pathways into the major ocean basins (Nicholls et al., 2009; Solodoch et al., 2022).

We also agree that narrow topographic passages are important for the redistribution of abyssal waters within the Atlantic. Observations and regional high-resolution modeling identify the Vema Channel as a major pathway for northward AABW transport between the Argentine and Brazil basins, while the Romanche and related fracture zones provide important routes for AABW crossing the Mid-Atlantic Ridge (Mercier et al., 1994; Frey et al., 2019; Tarakanov et al., 2020). However, the basin-scale and zonal-mean diagnostics used here do not isolate the individual contribution of each narrow passage to the Atlantic-wide upward penetration. Quantifying these contributions would require regional source tagging or dedicated section-based transport budgets, which are beyond the scope of the present basin-comparative analysis.

We have therefore added an explicit discussion of marginal-sea formation/export and topographically constrained overflow pathways. The added text now reads:

> *"Marginal seas and narrow topographic passages provide an additional regional context for the basin-scale return structure diagnosed here. Around Antarctica, the Weddell and Ross Seas are major sites of dense-water formation and export, and previous observational and tracer studies show that waters formed in different Antarctic sectors follow distinct pathways into the Atlantic, Indian, and Pacific basins (Nicholls et al., 2009; Solodoch et al., 2022). The enhanced ventilation thickness diagnosed in the Weddell sector is consistent with strong bottom-water influence within this formation–recirculation–export system. However, because the present CART experiment tags the global model bottom layer uniformly, it does not separate locally formed bottom water from recirculated or exported bottom-water signals within individual marginal seas. Narrow topographic passages likewise organize abyssal redistribution within the Atlantic. The Vema Channel provides a major pathway for northward AABW transport between the Argentine and Brazil basins, while the Romanche and associated fracture zones provide important routes for bottom water crossing the Mid-Atlantic Ridge (Mercier et al., 1994; Frey et al., 2019; Tarakanov et al., 2020). These pathways may contribute to the regional organization of the Atlantic bottom-water signal, but their individual contributions to the basin-scale upward penetration diagnosed here cannot be isolated from the present zonal-mean and globally tagged diagnostics. Regional source-tagging or section-based transport analyses would be required for such attribution."*

6. The classification thresholds in the regime analysis (Figure 5c–d) appear arbitrary

The authors define four dynamical-tracer regimes using a concentration threshold of C=0.25 and a diapycnal velocity threshold of $|\omega_d|=10^{-6}$ m /s. However, no justification is provided for these specific values:

1. Why 0.25 rather than 0.2 or 0.3? Does this threshold reflect a physical separation (e.g., a distinct mode in the joint distribution of C and ω_d), or is it chosen for convenience?

2. The velocity threshold of 10^{-6} m/s (~3 cm/day) is relatively high for abyssal diapycnal motions. What fraction of grid points is excluded by this threshold? If the authors have tested alternative thresholds, they should report the sensitivity. If not, they should at least acknowledge the arbitrary nature of the classification and interpret the percentages (e.g., Region 1 occupies 44.8% of the area) with appropriate caution.

Response: Thank you for this important comment. We agree that the thresholds used in the regime analysis should be described more clearly and should not be interpreted as uniquely defined physical boundaries. The purpose of the classification in Fig. 5c–d is to provide an operational diagnostic of where substantial bottom-water influence coincides with pronounced upward or downward diapycnal motion, rather than to identify objectively determined dynamical regimes.

The concentration threshold of $C = 0.25$ was selected from the spatial distribution of bottom-water concentration on the $\gamma^n = 28.1\ \mathrm{kg\,m^{-3}}$ surface. At this value, the classification captures the core regions of elevated bottom-water influence, particularly across the Southern Ocean, while separating them from the broader surrounding field with weaker concentration. To make this basis transparent, we have added Supplementary Fig. S7 showing the concentration distribution together with the $C = 0.25$ contour. We emphasize that $C = 0.25$ is an operational threshold rather than a unique physical separation in the concentration field.

The velocity threshold of $|\omega_d| = 10^{-6}\ \mathrm{m\,s^{-1}}$ was similarly selected from the diapycnal-velocity distribution shown in Fig. 2a to distinguish pronounced upward or downward motion from weaker background exchange. Locations without valid C or ω_d values are excluded before the classification and are not included in the reported valid-point or valid-area fractions. Grid points satisfying $|\omega_d| \leq 10^{-6}\ \mathrm{m\,s^{-1}}$, including the threshold boundaries, are treated as weak-motion regions and are not assigned to the four regimes. We have now quantified the extent of this excluded weak-motion range: it contains 48.1% of the valid grid points and 46.7% of the valid area on the $\gamma^n = 28.1\ \mathrm{kg\,m^{-3}}$ surface.

We have not treated $C = 0.25$ and $|\omega_d| = 10^{-6}\ \mathrm{m\,s^{-1}}$ as objectively determined critical values, and no formal alternative-threshold sensitivity analysis was used to define these regimes. Following the reviewer's suggestion, we have instead clarified the empirical basis and operational nature of the classification and have tempered the interpretation of the resulting areal percentages. In particular, the previously reported 44.8% refers to the fraction of the classified area occupied by Region1, rather than 44.8% of the entire valid density surface.

The revised description of the regime classification now reads:

> *"We classify the valid grid points into four diagnostic regimes using operational thresholds of $C = 0.25$ and $|\omega_d| = 10^{-6}\ m\,s^{-1}$ (Fig. 5c). The concentration threshold is selected from the spatial distribution of C on this density surface, where $C = 0.25$ provides a practical separation*

between the core regions of elevated bottom-water influence and the surrounding weaker-concentration field (Supplementary Fig. S7). The velocity threshold is selected from the corresponding diapycnal-velocity distribution (Fig. 2a) to distinguish pronounced upward or downward diapycnal motion from weaker background exchange. These thresholds are intended as operational diagnostic criteria rather than uniquely defined physical boundaries. Grid points with $|\omega_d| \leq 10^{-6}\, m\, s^{-1}$ *are treated as weak-motion regions and are not assigned to the four regimes; these account for 48.1% of the valid grid points and 46.7% of the valid area on this density surface."*

We have also clarified the interpretation of the Region 1 area fraction. The revised text now reads:

"The spatial distribution of these regimes (Fig. 5d) shows that Region 1 is not confined to isolated diapycnal velocity hotspots but occupies broad portions of the classified area on the $\gamma^n = 28.1\, kg\, m^{-3}$ *surface. Under the adopted operational thresholds, Region 1 accounts for 44.8% of the total area assigned to the four classified regimes."*

To emphasize the threshold dependence of these quantitative fractions, we added the following statement:

"Because the exact regime boundaries and associated areal fractions depend on the adopted operational thresholds, these percentages are interpreted as descriptive measures of the regime partition rather than uniquely defined physical proportions."

The revised description of panels c–d in the Fig. 5 caption now reads:

"(c) Schematic classification of four dynamical–tracer regimes using operational thresholds of $C = 0.25$ *and* $|\omega_d| = 10^{-6}\, m\, s^{-1}$*, separating relatively strong or weak bottom-water influence and pronounced upward or downward diapycnal motion. (d) Global distribution of the four regimes on the* $\gamma^n = 28.1\, kg\, m^{-3}$ *surface. White areas denote weak-motion regions with* $|\omega_d| \leq 10^{-6}\, m\, s^{-1}$ *or locations without valid values required for the classification; invalid locations are excluded from the reported area fractions."*

We further added Supplementary Fig. S7 to show the concentration field underlying the choice of $C = 0.25$. The caption reads: The Supplementary Fig. S7 and its caption are shown below:

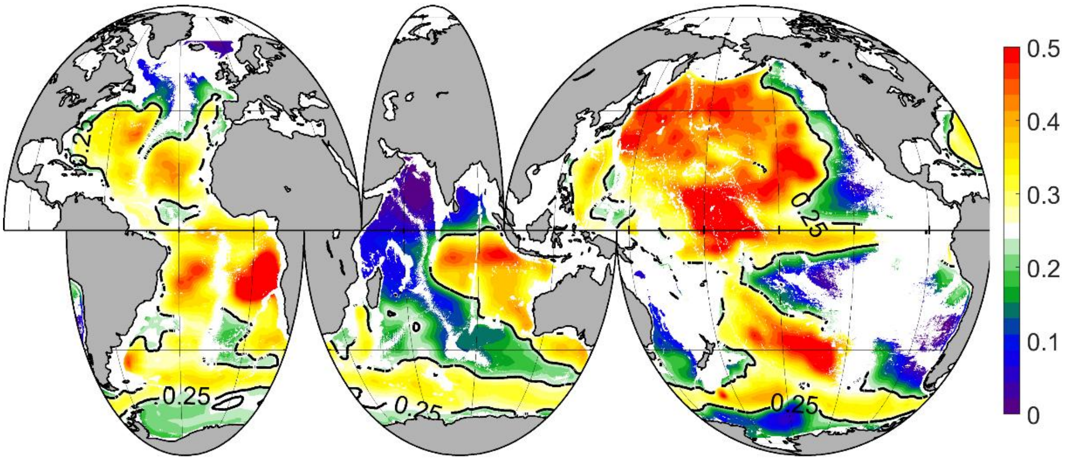

"Figure S7. Bottom-water-origin concentration on the $\gamma^n = 28.1\ kg\ m^{-3}$ *neutral-density surface, sampled from annual-mean fields at the location-specific diagnostic times selected by the concentration-tendency criterion in Sect. 2.1 of the main text. The mapped field therefore combines values sampled at location-specific diagnostic times rather than representing a snapshot at a common CART integration year. Concentration is dimensionless. The black contour marks* $C = 0.25$*, the operational division between higher- and lower-concentration regions in the regime classification in Fig. 5c–d. The map shows the spatial concentration pattern used for this classification."*

7. Minor inconsistencies in terminology and presentation

1. **Line 191** and **Section 3.1**: The authors refer to "30-year mean" diapycnal velocity in Figures 2b–e, but the CART simulation was integrated for 100 years under monthly climatological forcing. If the forcing is climatological (i.e., repeating annual cycle), what does a "30-year mean" refer to? Does it mean years 30–60 of the integration, or is it a time average over the last 30 years of the 100-year run? This needs clarification for all time-averaged fields (Figures 4, 5, and 6).

Response: Thank you for pointing out this ambiguity. We agree that the original use of "30-year mean" could incorrectly suggest that the diapycnal velocity was averaged over a selected 30-year period of the 100-year CART integration. This is not the case. The diapycnal-velocity diagnosis is independent of the CART integration. Both calculations are based on climatological fields constructed from the GLORYS12 reanalysis over 1994–2022, whereas the 100 years refer only to the diagnostic integration of the CART tracer equations under the repeated climatological forcing. We have therefore removed the term "30-year mean" throughout the manuscript and clarified the temporal basis of the diagnostics.

The corresponding methodological description now reads:

"For this study, monthly climatological temperature, salinity, and velocity fields were constructed from the GLORYS12 reanalysis over the period 1994–2022. These climatological fields were then used as the input for the CART experiment and for the diapycnal-velocity diagnosis described below."

Accordingly, the revised Fig. 2 caption now states:

"Figure 2 Diapycnal velocity ($m\,s^{-1}$) as a diagnostic of global ocean diapycnal motion. (a) Global distribution of diapycnal velocity diagnosed from the 1994–2022 GLORYS12 climatological fields on the neutral-density surface $\gamma^n = 28.1\ kg\ m^{-3}$ ... (b–e) Zonal-mean distributions of diapycnal velocity diagnosed from the 1994–2022 GLORYS12 climatological fields in the global ocean, Atlantic Ocean, Pacific Ocean, and Indian Ocean. Together, these panels illustrate the large-scale spatial organization of cross-isopycnal exchange in the global overturning circulation."

The corresponding text in Sect. 3.1 now reads:

"Having established the horizontal localization of abyssal diapycnal exchange, we next examine its large-scale vertical and basin-scale organization using the zonal-mean climatological diapycnal velocity fields shown in Fig. 2b–e."

We have also clarified the temporal basis of the CART-derived fields. Annual-mean concentration and water-age fields are obtained for each CART integration year, and the local quasi-equilibrium time is identified from the concentration-tendency criterion described in Sect. 2.1. Figure 4 uses the annual-mean concentration corresponding to this locally diagnosed quasi-equilibrium time.

To make the temporal basis of Fig. 4 explicit, the revised caption now reads:

"Figure 4 Zonal-mean distributions of bottom-water tracer concentration sampled at the local diagnostic times defined in Sect. 2.1 in the (a) global ocean, (b) Atlantic Ocean, (c) Pacific Ocean, and (d) Indian Ocean."

Figure 5 combines this concentration field with the climatological diapycnal-velocity diagnosis to calculate the concentration-weighted diapycnal transport. Figure 6 uses the corresponding annual-mean water-age field evaluated at the same locally diagnosed time. Thus, none of Figs. 4–6 represents an average over a prescribed 30-year subset of the 100-year CART integration.

2. **Line 240**: The phrase "initial stages (years 1 and 10)" is used to describe ventilation thickness evolution. Since the forcing is climatological, "years" here refer to integration steps rather than calendar years. The authors should explicitly state this to avoid confusion with actual temporal evolution in the real ocean.

Response: Thank you for pointing this out. We agree that the use of "years" in the original text could be confused with calendar years or actual temporal evolution in the ocean. The 100-year CART experiment is conducted under repeated climatological forcing, and years 1–100 therefore refer to diagnostic integration years rather than calendar years. We have clarified this terminology in the Methods and consistently revised the corresponding descriptions of the ventilation-thickness evolution.

The corresponding methodological description now reads:

> *"Using these initial and source-layer conditions, the CART equations are integrated continuously for 100 years under the monthly climatological forcing derived from GLORYS12. Here, the 100-year period denotes the model integration time under the climatological forcing rather than 100 calendar years of transient ocean evolution. The diagnosed ages measure elapsed time for the tagged component under the repeated climatological annual cycle."*

The revised Fig. 3 caption now reads:

> *"Figure 3 Global distribution of bottom-water ventilation thickness (m) at CART integration years (a) 1, (b) 10, (c) 50, and (d) 100."*

The corresponding Results text now reads:

> *"As a column-integrated diagnostic, ventilation thickness provides a compact view of where abyssal return first emerges, how broadly it expands, and where it is expressed most strongly through the full water column. Its evolution at CART integration years 1, 10, 50, and 100 is shown in Fig. 3."*

The subsequent description has been revised consistently:

> *"During the initial stages of the CART integration (integration years 1 and 10; Fig. 3a, b), ventilation thickness remains relatively weak and spatially patchy, with the more prominent signals occurring in the Southern Ocean and in a limited number of boundary-associated regions."*

and

> *"By integration years 50 and 100 (Fig. 3c, d), the ventilated footprint expands across all major basins while remaining strongly heterogeneous."*

3. **Line 415**: The statement "the Pacific acts as the principal reservoir of old bottom waters" is supported by the age field, but the concentration field (Figure 4c) shows that bottom-water influence in the Pacific is largely confined to the deepest density classes. This does not necessarily mean the Pacific is a reservoir—it could simply reflect weak diapycnal mixing there. The authors might consider a more nuanced wording that distinguishes "storage" from "lack of transformation."

Response: Thank you for this helpful comment. We agree that describing the Pacific as a "reservoir" could imply storage that is not directly established by the concentration and age diagnostics. Figure 4c primarily shows that bottom-water influence remains confined to the deeper density classes over much of the Pacific, indicating comparatively limited upward penetration, whereas the age field shows slower renewal and older bottom-water signals. We have therefore revised the wording to distinguish these two aspects and to avoid interpreting deep confinement as evidence of storage.

The corresponding Results text associated with Fig. 4c now reads:

> *"Broad confinement to deep density classes and localized equatorial ascent indicate comparatively limited upward penetration of bottom-water influence across much of the Pacific, with only selected pathways providing more efficient ascent toward lighter density classes (Shah et al., 2017; Talley, 2013; Tamsitt et al., 2017)."*

We have also revised the basin-scale synthesis accordingly. The corresponding text now reads:

> *"The concentration and age fields reveal related spatial contrasts:: the Southern Ocean dominates the large-scale return of bottom-water influence, the Atlantic supports the strongest upward penetration but with substantial northward aging, the Pacific shows older bottom-water signals together with comparatively limited upward penetration, and the Indian Ocean contains more localized return corridors."*

Recommendation

The manuscript presents a valuable global diagnostic exercise, but the issues outlined above—particularly the lack of clarity in the CART implementation, the mismatch between the conceptual model and the results, and the over-interpretation of climatologically forced age fields—need to be addressed. I recommend **major revision**. I encourage the authors to provide a more transparent description of their numerical methods and to temper their claims about the absolute timescales in light of the forcing simplifications.

Response: We thank the reviewer for this overall recommendation. The principal concerns summarized here have been addressed through the revisions described in our response to the General Comments and in the detailed responses above.

References cited in this response

Deleersnijder, E., Campin, J.-M., and Delhez, E. J. M.: The concept of age in marine modelling I. Theory and preliminary model results, J. Mar. Syst., 28, 229–267, https://doi.org/10.1016/S0924-7963(01)00026-4, 2001.

Frey, D. I., Morozov, E. G., Fomin, V. V., Diansky, N. A., and Tarakanov, R. Y.: Regional Modeling of Antarctic Bottom Water Flows in the Key Passages of the

Atlantic, J. Geophys. Res.-Oceans, 124, 8414–8428, https://doi.org/10.1029/2019JC015315, 2019.
Large, W. G., McWilliams, J. C., and Doney, S. C.: Oceanic vertical mixing: A review and a model with a nonlocal boundary layer parameterization, Rev. Geophys., 32, 363–403, https://doi.org/10.1029/94RG01872, 1994.
Mercier, H., Speer, K. G., and Honnorez, J.: Flow pathways of bottom water through the Romanche and Chain Fracture Zones, Deep-Sea Res. Pt. I, 41, 1457–1477, https://doi.org/10.1016/0967-0637(94)90055-8, 1994.
Nicholls, K. W., Østerhus, S., Makinson, K., Gammelsrød, T., and Fahrbach, E.: Ice–ocean processes over the continental shelf of the southern Weddell Sea, Antarctica: A review, Rev. Geophys., 47, RG3003, https://doi.org/10.1029/2007RG000250, 2009.
Shah, S. H. A. M., Primeau, F. W., Deleersnijder, E., and Heemink, A. W.: Tracing the Ventilation Pathways of the Deep North Pacific Ocean Using Lagrangian Particles and Eulerian Tracers, J. Phys. Oceanogr., 47, 1261–1280, https://doi.org/10.1175/JPO-D-16-0098.1, 2017.
Solodoch, A., Stewart, A. L., Hogg, A. McC., Morrison, A. K., Kiss, A. E., Thompson, A. F., Purkey, S. G., and Cimoli, L.: How Does Antarctic Bottom Water Cross the Southern Ocean?, Geophys. Res. Lett., 49, e2021GL097211, https://doi.org/10.1029/2021GL097211, 2022.
Talley, L.: Closure of the Global Overturning Circulation Through the Indian, Pacific, and Southern Oceans: Schematics and Transports, Oceanography, 26, 80–97, https://doi.org/10.5670/oceanog.2013.07, 2013.
Tamsitt, V., Drake, H. F., Morrison, A. K., Talley, L. D., Dufour, C. O., Gray, A. R., Griffies, S. M., Mazloff, M. R., Sarmiento, J. L., Wang, J., and Weijer, W.: Spiraling pathways of global deep waters to the surface of the Southern Ocean, Nat. Commun., 8, 172, https://doi.org/10.1038/s41467-017-00197-0, 2017.
Tarakanov, R. Y., Morozov, E. G., and Frey, D. I.: Hydraulic Continuation of the Abyssal Flow From the Vema Channel in the Southwestern Part of the Brazil Basin, J. Geophys. Res.-Oceans, 125, e2020JC016232, https://doi.org/10.1029/2020JC016232, 2020.